JOURNAL OF GEOPHYSICAL RESEARCH, VOL. 112, C07019, doi:10.1029/2006JC003982, 2007

Evaluation of ocean models using observed and simulated drifter trajectories: Impact of sea surface height on synthetic profiles for data assimilation

Charlie N. Barron,[1] Lucy F. Smedstad,[1] Jan M. Dastugue,[1] and Ole Martin Smedstad[2]

Received 18 October 2006; revised 11 January 2007; accepted 13 March 2007; published 17 July 2007.

[1] The impact of global Navy Layered Ocean Model (NLOM) sea surface height (SSH) on global Navy Coastal Ocean Model (NCOM) nowcasts of ocean currents is investigated in a series of experiments. The studies focus on two primary aspects: the role of NLOM horizontal resolution and the role of differences between the SSH means in NLOM and the Modular Ocean Data Assimilation System (MODAS) climatology. To evaluate the impact of changes to the assimilation system, we compare observed drifter trajectories with trajectories simulated using global NCOM over 7-day timescales. The results indicate general improvement in NCOM currents as a result of increasing NLOM horizontal resolution. The effects of accounting for the differences between NLOM and MODAS mean that SSH is less clear, with some regions showing a decline in simulation skill while others show improvement or little impact. These outcomes supported recommendations for operational transition to 1/32° global NLOM with continued refinement to methods accounting for differences in mean SSH.

Citation: Barron, C. N., L. F. Smedstad, J. M. Dastugue, and O. M. Smedstad (2007), Evaluation of ocean models using observed and simulated drifter trajectories: Impact of sea surface height on synthetic profiles for data assimilation, *J. Geophys. Res.*, *112*, C07019, doi:10.1029/2006JC003982.

1. Introduction

[2] Different ocean modeling system formulations are evaluated by comparing simulated drifter trajectories using model currents with corresponding independent drifter observations. Time-integrated near-surface movement of water from one location to another is naturally measured through Lagrangian drifters. Numerous studies use sets of drifters to identify climatological circulation patterns and modes of variability [*Poulain*, 1999; *Fratantoni*, 2001; *Reverdin, et al.*, 2003; *Zhurbas and Oh*, 2003]. Others develop more comprehensive climatological depiction by supplementing actual drifter observations with trajectories simulated in numerical models. *Lugo-Fernandez et al.* [2001] used real and simulated drifters as a proxy for dispersal of coral larvae from the Flower Garden Banks. *Naimie et al.* [2001] combines 3 years of observations from 155 drifters with trajectories simulated by a climatologically and tidally forced model. The resulting data set averages 680 observational days of measured trajectories per month. Statistics from these data are compared with results based on simulated monthly drifter deployments in the model. Many differences between the model and observational records are linked to episodic wind events not represented in the climatological forcing. Similar errors in daily forecasts arise from atmospheric events poorly resolved or otherwise not represented by the global atmospheric models. Studies also use observed trajectories to validate predictions of surface currents. *Vastano and Barron* [1994] evaluate 24-hour trajectories based on surface circulation determined by tracking features in satellite imagery, while *Thompson et al.* [2003] examine simulated trajectories up to 100 hours on the shelf off Nova Scotia.

[3] Accuracy of drifter-based estimates of water movement depends upon the accuracy in determining the location of a drifter and the slip of the drifter relative to the actual water movement at the drifter location. *Hansen and Herman* [1989] found that for the commonly used drifters with 10 or 30 m "window shade" drogues, at best, a daily mean velocity accuracy of 2–3 cm s^{-1} could be expected, with the standard rate of Argos communications from two satellites, within the 5 cm s^{-1} Tropical Ocean Global Atmosphere (TOGA) standard. By attaching neutrally buoyant current meters to the top and bottom of 15 m holey sock and TRISTAR drogues, *Niiler et al.* [1995] found slippage errors of 0.5–3.5 cm s^{-1}. While careful reprocessing can reduce errors below 0.5 km/day, the typical 2- to 3.5 cm s^{-1} errors in the daily mean current are equivalent to a separation error of 1–3 km day^{-1}, with a 4.3 km day^{-1} error equivalent to the TOGA standard.

[4] The predictability of drifter trajectories depends not only on the accuracy with which drifters represent water parcel advection but also, often more importantly, on the dispersion of closely spaced water parcels, a process which may not be resolved on the space and timescales sampled by

[1]Naval Research Laboratory, Stennis Space Center, Mississippi, USA.
[2]Planning Systems Incorporated, Stennis Space Center, Mississippi, USA.

0148-0227/07/2006JC003982$09.00

Table 1. Numerical and Observational Error Estimates for Predicting Drifter Trajectories[a]

Region	σ_v, cm s^{-1}	RMS Prediction Error After 3 Days, km	RMS Prediction Error After 7 Days, km
Numerical results from the work of *Özgökmen et al.* [2000]			
Gyre interior	2.8	0.4	1.7
Western boundary	12	3.0	10.9
Midlatitude jet	28	14.6	67.4
Observational (tropical Pacific) results from the study of *Özgökmen et al.* [2001]			
Cluster I	24	7	10
Cluster II	31	10	15
Cluster III	54	20	65

[a]The numerical results correspond to the minimum (0.25° × 0.25°) spacing of simulated drifters. The observational results correspond to the prediction error using the maximum 6-hourly data assimilation during the first 7 days after deployment, the period of maximum cluster density.

the observations or models to be evaluated. Even if a model accurately represents ocean velocity, the model's discrete sampling of the ocean will lead to differences in the simulated trajectories. As the distance between predicted and true drifter position increases, the trajectories sample increasingly uncorrelated environmental conditions that tend to increase separation distance.

[5] Predictability of Lagrangian trajectories has been examined using observed and modeled drifters. A model study by *Özgökmen et al.* [2000] indicates that error in predicted drifter position tends to increase over time at a rate proportional to σ_V, the square root of the velocity variance σ_V^2, where the velocity variance is the sum of the variances of the east (u) and north (v) velocity components, $\sigma_V^2 = \sigma_u^2 + \sigma_v^2$. The variances are calculated relative to a spatial and temporal mean. Uniformly seeded drifters in an idealized double-gyre circulation model are sampled in three domains: the gyre interior, the western boundary current, and the midlatitude jet. Drifter velocities are predicted as a linear combination of the velocities of neighboring particles weighted by the expected covariance. Sampling at higher density reduces the distance between the modeled trajectory and its nearest neighbors, thereby increasing the skill of predictions that assimilate neighboring trajectories. Table 1 shows their numerical results at the highest sampling density of 0.25° × 0.25°. Observational results from the study of *Özgökmen et al.* [2001] are included in Table 1 as well. This subsequent study uses three clusters of World Ocean Circulation Experiment (WOCE) drifters in the tropical Pacific, clusters that are within 5° latitude of the equator and are distinct from the gyre regions in the prior examination. Various methods are investigated to predict drifter trajectories; the results considered here are from the method determined to be most accurate, predicting a drifter trajectory using a Kalman filter to assimilate 6-hourly velocities sampled from the other cluster members. For the highest-density clusters immediately after deployment, root mean square (RMS) prediction errors for the assimilative method remained $\leq$15 km for about 7 days for the first two, less energetic clusters (σ_V between 24 and 31 cm s^{-1}); RMS error in the more energetic (σ_V = 54 cm s^{-1}) third cluster grew to 20 km by the fourth day and exceeded 65 km by day 7. These studies provide a drifter predictability baseline error that is roughly proportional to the square root of velocity variance. When evaluating drifter trajectories simulated by a model, errors inherent in predicting Lagrangian trajectories are compounded by errors in the model velocity field. Many comparisons with observations are needed to allow confidence in the conclusions of such a study.

[6] In this report, we evaluate the impact of model system modifications on surface circulation by regionally comparing simulated drifters with trajectories from a yearlong global set of Lagrangian observations. A description of the models is given in section 2, while section 3 provides an overview of the experiments. Data and methods are covered in section 4, and section 5 discusses the results.

2. Models

[7] As presented in the paper of *Rhodes et al.* [2002], the global ocean model suite developed by the U.S. Naval Research Laboratory (NRL) and run operationally by the U.S. Naval Oceanographic Office has three components: the Navy Layered Ocean Model (NLOM), the Modular Ocean Data Assimilation System (MODAS), and the Navy Coastal Ocean Model (Figure 1). This NRL Global Ocean Modeling System (NGOMS) endeavors to make more efficient use of operational computational resources by leveraging the strengths and capabilities of the system elements. Different NGOMS formulations are evaluated by comparing simulated drifter trajectories using NCOM currents with independent drifter observations.

[8] Designed to provide high-fidelity forecasts of deepwater front and eddy location, global NLOM emphasizes high horizontal resolution at the expense of coarse (seven-layer) vertical resolution and coverage only for sub-Arctic regions deeper than 200 m [*Wallcraft et al.*, 2003]. NLOM must maintain all of its layers at nonzero thickness throughout its domain, a consequence of approximations that greatly increase computational efficiency. Thus its layers must neither surface nor intersect bottom topography, leading to the deepwater restriction. The original operational global NLOM in NGOMS V2.0 [*Smedstad et al.*, 2003] was configured with 1/16° midlatitude horizontal resolution; for the upgrade to NCOMS V2.5, NLOM horizontal resolution has been increased to 1/32° [*Shriver et al.*, 2007].

[9] Global NCOM extends over continental shelves, coastal regions, and the Arctic, providing global coverage with minimum bottom depth of 5 m. Described in detail by *Barron et al.* [2006], global NCOM maintains fairly high vertical resolution using 40 logarithmically stretched material levels in the vertical: 19 terrain-following sigma levels in the upper 141 m or shallower over 21 z levels extending to a maximum 5500-m depth. The uppermost level has a rest thickness of 1 m in the open ocean. *Barron et al.* [2004] and *Kara et al.* [2006] evaluate nonassimilative and NGOMS 2.0 versions of global NCOM through comparisons with unassimilated ocean observations including surface observations of height (SSH), temperature (SST), and salinity and subsurface observations of mixed layer depth, temperature, and salinity. While global NCOM has relatively high vertical resolution, its horizontal resolution is limited to 1/8° to fit within the limits of its operational computational resources. On this relatively coarse grid, NCOM is

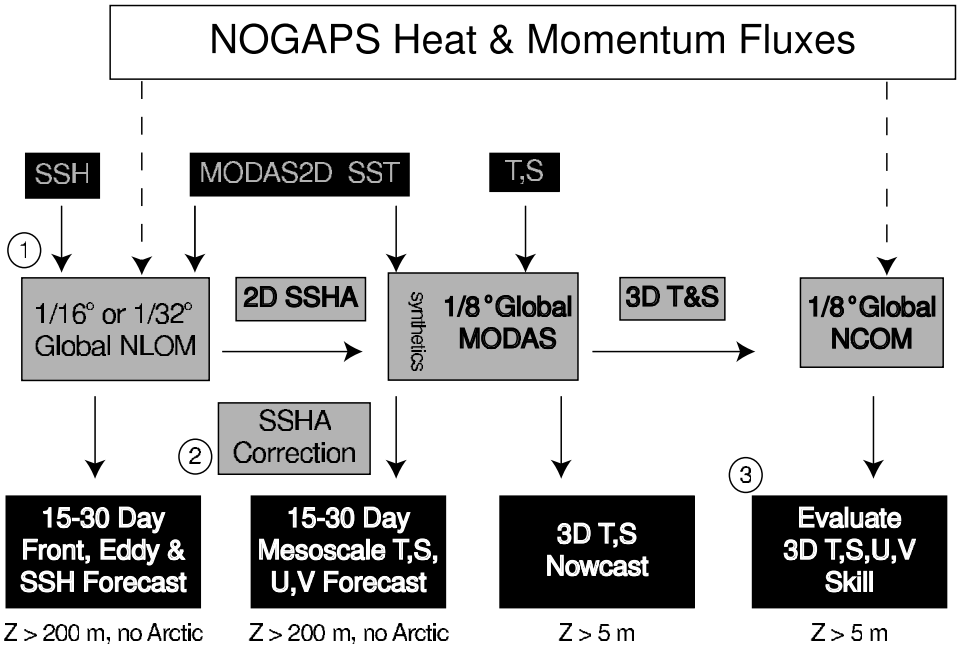

Figure 1. Wiring diagram of the NRL Global Ocean Modeling System, adapted from the work of *Rhodes et al.* [2002], showing the relationship between NLOM, MODAS, and NCOM. Two numbered elements indicate modifications to the standard configuration, which are evaluated in this article: (1) changing the resolution of global NLOM from 1/16° to 1/32° and (2) accounting for the difference between the NLOM and MODAS SSHA. Rectangle (3) indicates the global NCOM results evaluated in this study. NGOMS V2.0 uses the 1/16° NLOM, while V2.5 incorporates NLOM at 1/32°.

eddy-permitting but only marginally eddy-resolving, lacking the horizontal resolution needed to robustly forecast the longer-term dynamic evolution of mesoscale fronts and eddies [*Hurlburt and Hogan*, 2000]. Through assimilation, NCOM is able to maintain a reasonably accurate representation of fronts and eddies, and it thereby adequately provides boundary conditions for higher-resolution nested models.

[10] The assimilation that leverages the high horizontal resolution of NLOM and that allows the extended coverage of NCOM must allow the global system to complete daily integrations within limited operational computational constraints. While more sophisticated variational techniques are under investigation to improve solution accuracy, a simple, low-cost relaxation has been initially used for the time-critical operational system. In this system, SSH is not assimilated directly but is instead used to derive profiles of temperature and salinity for assimilation. SST from the global MODAS-2D analysis [*Barron and Kara*, 2006] and the sea surface height anomaly (SSHA) from global NLOM are projected in the vertical using the MODAS dynamic climatology [*Fox et al.*, 2002] to make three-dimensional fields of temperature and salinity. Note that salinity is determined from temperature using local climatological T-S curves; if estimates of surface salinity were available, these would be used to produce more accurate salinity profiles. Blended in the Arctic with the monthly Generalized Digital Environmental Model (GDEMV 3.0) [*Teague et al.*, 1990] climatology, the resulting global temperature and salinity files are assimilated at each time step into the NCOM solution using slow data insertion,

$$T(x,y,z,t) = (1 - a(z))T_{\mathrm{N}}(x,y,z,t) + a(z)T_{\mathrm{M}}(x,y,z,t) \quad (1)$$

$$a(z) = \left(2\Delta t/\tau\right)\left(1 - e^{-\left|z/b\right|}\right) \quad (2)$$

where T is the post-assimilation temperature (or salinity), T_{N} is the NCOM result before assimilation, and T_{M} is the MODAS temperature (or salinity) interpolated to time t, depth z, and horizontal location x, y. The assimilation weight for each time step $a(z)$ depends on the ratio of the time step Δt to the relaxation timescale τ and the ratio of the grid point depth z to the relaxation depth scale b. For the results in this study, b is 200 m, Δt is 5 min, and τ is 48 hours.

3. Experiments

[11] The experiments evaluated in this study focus on the use of high-resolution SSH fields from NLOM within 1/8° global MODAS to produce synthetic temperature and salinity profiles for assimilation into global NCOM. The experiments have two variables: the version of NLOM used to calculate SSH, and the optional inclusion of a correction term that accounts for systematic differences between NLOM and MODAS anomalies. As indicated by label (1) in Figure 1, the high-resolution SSH for MODAS is

produced by either 1/16° or 1/32° global NLOM. However, MODAS does not use the total NLOM SSH; MODAS expects the SSH it provided to be equivalent to an offset from the steric height anomaly relative to 1000 m in the MODAS hydrographic climatology [*Boebel and Barron*, 2003]. In general, the SSH observed by altimeters or simulated in an ocean model is a combination of steric and nonsteric components; *Shriver and Hurlburt* [2000] find that the nonsteric component contributes over 50% of the total SSH variability for more than 37% of the global ocean. They also describe how the abyssal pressure anomaly can be used to determine SSHN, the nonsteric contribution to SSH. Subtracting the nonsteric SSHN from the total SSH produces SSHB, a steric (sometimes referred to a baroclinic) component of the NLOM SSH. The NLOM estimate for steric SSH anomaly is calculated by $SSHA_{NLOM} = SSHB - \overline{SSHB}$, where $\overline{SSHB}$ is the long-term mean of SSHB at each point. The SSHA provided to MODAS to calculate temperature and salinity profiles is given by

$$SSHA = SSHB - \overline{SSHB} + (SSHA_{MODAS} - SSHA_{NLOM}). \quad (3)$$

The SSHA correction term $(SSHA_{MODAS} - SSHA_{NLOM})$ is designated (2) in Figure 1. We approximate the SSHA correction using the difference between $\overline{SSHB}$ from the 1/16° NLOM and the climatological MODAS steric height anomaly integrated from 2500 m or the bottom to the surface. The SSHA from equation 3 is used with the MODAS SST analysis to derive temperature and salinity profiles for NCOM assimilation as described above.

[12] Table 2 indicates the experiments examined in this report. The control experiment is the original operational three-component NGOMS V2.0 with 1/16° global NLOM and no $(SSHA_{MODAS}-SSHA_{NLOM})$ correction term. We would like to determine whether some alternative formulations lead to improved system performance. Such a determination requires a broad validation study examining many aspects of the model results; results of such a study were reported in the paper of *Barron et al.* [2004] and *Kara et al.* [2006] for V2.0. To support an upgrade decision, similar evaluations have been made using the alternative model system formulations. This paper focuses on one aspect of a comprehensive system validation study: the accuracy of predicted drifter trajectories.

[13] What are the system alternatives, and why do we expect that these might be improvements? V2.0a uses the same model components but incorporates a SSH correction term that attempts to account for differences between the mean NLOM SSH and the mean MODAS SSH. We expect that by accounting for this difference, the MODAS will be able to project SST and NLOM SSH more accurately into synthetic temperature and salinity profiles. Assimilation of these more accurate profiles by global NCOM should increase the fidelity of model circulation and should lead to more accurate trajectory predictions. A different modification is incorporated in experiment V2.5, the second-generation operational NGOMS: $SSHA_{NLOM}$ from 1/16° NLOM is replaced with the 1/32° NLOM version. We expect that increasing NLOM resolution leads to a better representation of true SSH, thus leading to a more accurate distribution of temperature and salinity in the resulting MODAS profiles and finally more accurate circulation in global NCOM. V2.5a pairs the mean SSH correction term from V2.0a with the $SSHA_{NLOM}$ from 1/32° NLOM used in V2.5. Reference system performances are evaluated using a persistence case, which assumes that velocities are uniformly zero, and the clim case, which approximates drifter motion based on the 2000–2002 mean currents NCOM from V2.0 NGOMS.

Table 2. NRL Global Ocean Modeling System Experiments[a]

Experiment	SSHB	$\overline{SSHB}$	$(SSHA_{MODAS}-SSHA_{NLOM})$
V2.0	1/16° NLOM	1/16° NLOM	0
V2.5	1/32° NLOM	1/32° NLOM	0
V2.0a	1/16° NLOM	1/16° NLOM	Based on 1/16° NLOM
V2.5a	1/32° NLOM	1/32° NLOM	Based on 1/16° NLOM
Persist	No motion: Predicted position is always the initial location		
Clim	Motion using the mean 1998–2001 currents from V2.0		

[a]V2.0 is the original operational three-component NGOM system, while V2.5 is the second-generation version. $SSHA = SSHB - \overline{SSHB} - (SSHA_{MODAS} - SSHA_{NLOM})$.

[14] What are the impacts of assimilation and the SSHA correction term on the currents simulated by global NCOM? The NCOM fields evaluated are indicated by label (3) in Figure 1. Results for the Kuroshio east of Japan are shown in Figure 2. Assimilation of the MODAS profiles maintains tighter density gradients, transforming the weak Kuroshio extension simulated in the nonassimilative case (Figure 2a) into a much more robust, realistic current in NGOMS V2.5 (Figure 2b). The SSHA correction term (Figure 2c) indicates that the NLOM mean SSH is generally higher than the MODAS mean south of the Kuroshio, or, equivalently, that the $SSHA_{MODAS}$ in these areas is more positive than a corresponding $SSHA_{NLOM}$. Thus a height offset should be added to $SSHA_{NLOM}$ in these regions to produce a correct estimate of SSHA in computing a MODAS synthetic profile. Inclusion of the SSHA correction term strengthens density gradients and current speeds (Figure 2d), particularly near 165°E. Assimilation leads to a more realistic representation of the Kuroshio extension, and inclusion of the SSHA correction factor provides additional benefit.

[15] While assimilation of synthetic profiles generally brings NCOM into closer agreement with observed circulation conditions, results in the Alaska Stream (Figure 3) reflect dynamics inadequately represented in the present approach. In the nonassimilative global NCOM case, Figure 3a, a robust Alaska Stream is evident at 150 m, in agreement with historical observations [*Chen and Firing*, 2006]. Assimilation in NGOMS V2.5 (Figure 3b) and in NGOMS V2.0 (not shown) greatly reduces this current, indicating that the assimilated MODAS synthetic profiles in this experiment do not have the correct vertical structure. One contributing factor is the MODAS linkage between subsurface temperature and salinity. A halocline that is not correlated with a thermocline, a feature of the Alaska Stream [*Chen and Firing*, 2006], is not adequately represented by the MODAS approach, which estimates a temperature profile alone and then projects salinity as a function of temperature. A second difficulty arises if the location or

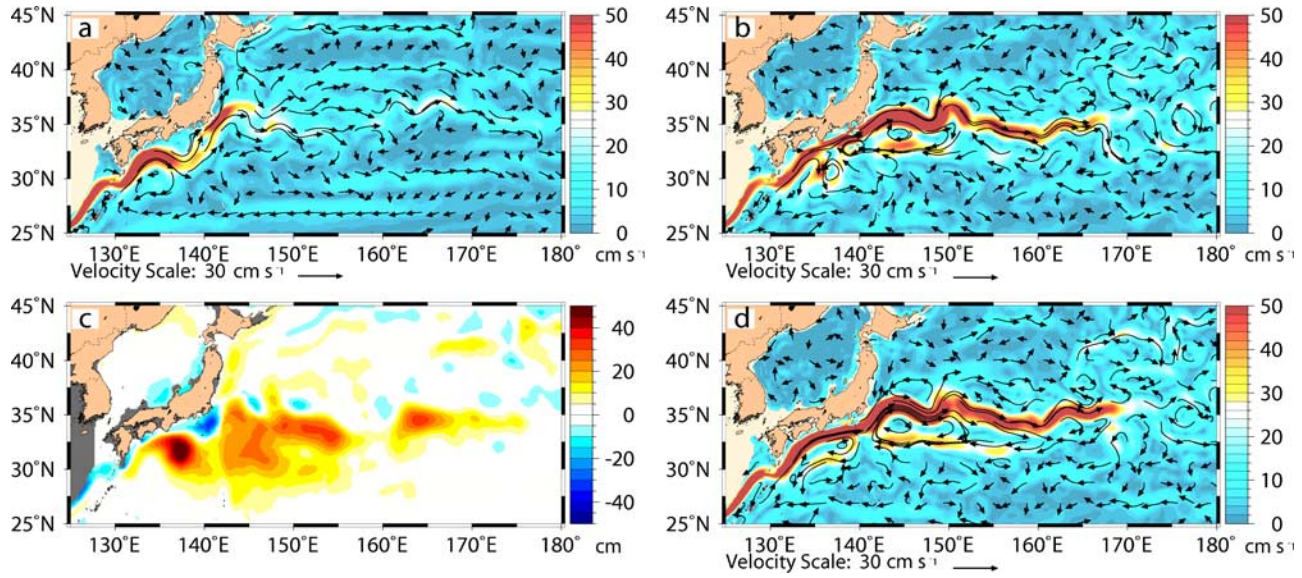

Figure 2. Impact of data assimilation and ($SSHA_{MODAS}$ − $SSHA_{NLOM}$) correction term in the Kuroshio region. Figures 2a, 2b, and 2d depict current vectors superimposed on current speed at 150 m depth from: (a) 1998–2000 nonassimilative global NCOM mean, (b) 2003 V2.5 NCOM mean, and (d) 2003 V2.5a NCOM mean. Figure 2c is the height correction term in centimeters to covert from V2.5 to V2.5a (or V2.0 to V2.0a). Assimilation produces tighter density gradients, transforming weak Kuroshio extension simulated in the nonassimilative case into a more robust, realistic current in V2.0. Inclusion of the SSHA correction term strengthens density gradients and current speeds, particularly near 165°E.

gradients of the front differ between NLOM and MODAS. The latter source of error is addressed by addition of the SSHA correction term, ($SSHA_{MODAS}$ − $SSHA_{NLOM}$), as shown in Figure 3c. In this case, the SSHB mean in NLOM is low relative to the MODAS mean, indicating that a more negative SSHA should be used to calculate synthetic profiles. While unable to address the halocline deficiency, the correction term in Figure 3c mitigates the assimilation

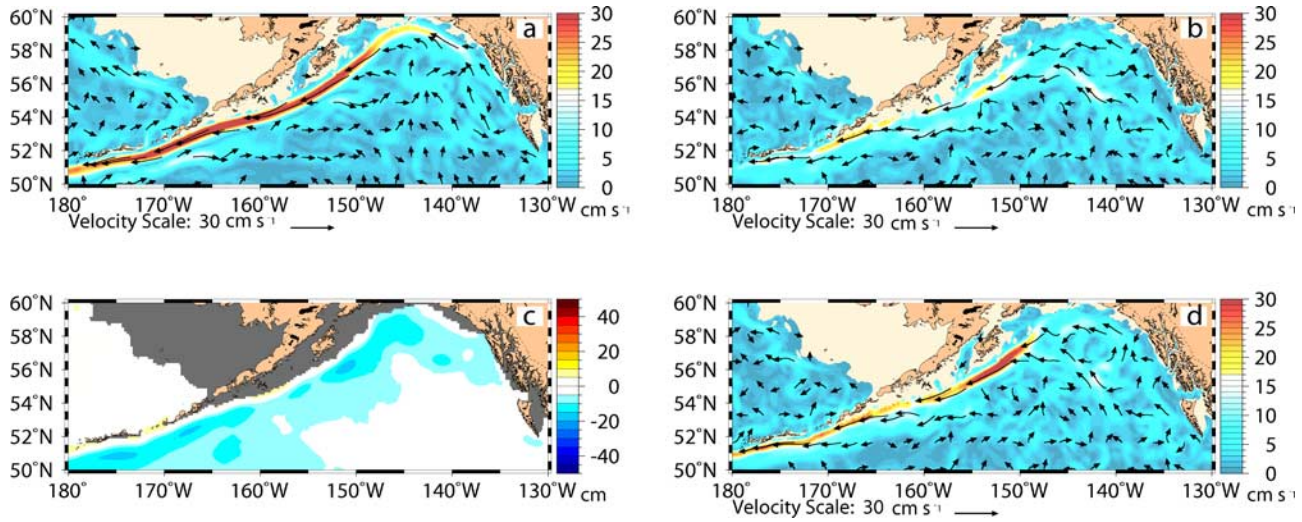

Figure 3. Impact of data assimilation and ($SSHA_{MODAS}$−$SSHA_{NLOM}$) correction term in the Alaska Stream region. Figures 3a, 3b and 3d depict current vectors superimposed on current speed at 150 m depth from: (a) 1998–2000 nonassimilative global NCOM mean, (b) 2003 V2.5 NCOM mean, and (d) 2003 V2.5a NCOM mean. Figure 3c is the height correction term in centimeters to covert from V2.5 to V2.5a (or V2.0 to V2.0a). Errors due to a nonzero ($SSHA_{MODAS}$−$SSHA_{NLOM}$) reinforce MODAS errors in representing haloclines uncorrelated with thermoclines, greatly weakening the Alaska Stream in V2.5. While not addressing the halocline deficiency, the correction term in Figure 3c mitigates the assimilation errors somewhat in Figure 3d and allows a more realistic depiction of the Alaska Stream.

errors in NLOM V2.5a (Figure 3d), leading to a more realistic representation of the Alaska Stream.

4. Data and Evaluation

[16] Numerous categories of validation metrics could be applied to assess the relative performance of the various model experiments. This article focuses on the use of observed and simulated drifter trajectories to evaluate relative model performance in Lagrangian movement of water. To do the evaluation, we simulate 7-day drifter trajectories initialized collocated with observed drifters. Our performance metric for each simulated drifter is its time-varying separation from its observed counterpart.

[17] Observed drifter trajectories are acquired from the National Oceanic and Atmospheric Administration (NOAA) Global Drifter Program (GDP). These data are accessible at www.aoml.noaa.gov/phod/dac/dacdata.html via the GDP Drifter Data Assembly Center. Interpolation of the WOCE-TOGA surface velocities to uniform 6-hour interval trajectories is described in detail by *Hansen and Poulain* [1996]. Details on the drifters and the processing of the drifter data may be found in the study of *Lumpkin and Pazos* [2007].

[18] Simulated trajectories are based on velocity fields archived from the model experiments for 2003 and are derived using a method adapted from the work of *Vastano and Barron* [1994]. Although the observed drifters have a drogue centered at 15 m depth, we opt for the surface velocity field because it was archived every 3 hours, while the interval between samples of the full three-dimensional velocity field was twice as long. Simulations are calculated in year 2003 for 30 selected regions (Table 3) of the global ocean. We also report σ_V for each region in Table 3 using the V2.0 NCOM time series to calculate velocity variance as a regional spatial and temporal mean value.

[19] In each region, we identify the locations of observed drifters at 0:00 UCT. Starting from these locations, we integrate the drifter trajectories over 7 days using a fourth-order Runge-Kutta method [*Press et al.*, 1986] with a 1-hour time step and multilinear time-space interpolation of the 3-hourly surface velocity fields.

[20] Examples of 7-day simulated and observed drifter trajectories are shown in Figure 4. Two panels (Figures 4a and 4b) show trajectories initialized on 10 December 2003. These plots reveal the irregular spatial and temporal sampling of the drifter observations and reflect an above-average number of drifters in these regions. For example, within the East Asian Pacific region, the Yellow Sea and central East China Sea tend to have fewer observations than does the Kuroshio between Taiwan and Japan. The latter two panels show a pair of drifters near the Gulf Stream off Cape Hatteras initialized on consecutive days, 24 January (Figure 4c) and 25 January (Figure 4d) 2003. Trajectory predictions for the northeastern drifter seem highly correlated between the 2 days, while predictions for the southwestern drifter would show very low correlation from 1 day to the next. We treat comparisons initialized on consecutive days from a common observed trajectory as independent observations, an assumption that is more valid in some (low-correlation) cases than in others.

Table 3. Latitude Range, Longitude Range, and σ_V for Regions Used in the Study

Region	Lat. Range	Long. Range	σ_V, cm s^{-1}
Agulhas	45°–25°S	0°–50°E	34
Australia-New Zealand	57°–18°S	145°E–170°W	25
Arabian Sea	5°S–35°N	30°–85°E	38
Eastern North Pacific	15°–65°N	170°–93°W	22
Benguela Current	35°S–0°N	0°–30°E	24
Black Sea	40°–47°N	25°–43°E	24
Brazil Malvinas Confluence	45°–5°S	60°–10°W	23
Celtic-Biscay-North Sea	47°–65°N	25°W–10°E	19
Central Pacific	10°–50°N	160°E–140°W	26
East Asian Pacific	5°–41°N	105°–135°E	34
Equatorial Atlantic	20°S–20°N	55°W–15°E	29
Equatorial Pacific	20°S–20°N	118°E–80°W	32
Gulf Stream	20°–45°N	85°–65°W	38
Gulf of Alaska	30°–62°N	180°–128°W	23
Gulf of Guinea	10°S–25°N	22°W–15°E	28
Gulf of Mexico	16°–31°N	98°–75°W	38
Humboldt Current	60°S–0°N	100°–60°W	21
Intra Americas Seas	5°–31°N	100°–55°W	33
Iberia Region	30°–47°N	20°W–0°E	19
Indian Ocean	30°S–25°N	20°–110°E	32
Java Sea	20°S–5°N	95°–145°E	32
Kuroshio	25°–45°N	125°–180°E	35
Madagascar	28°–10°S	40°–53°E	34
North Atlantic	0°–80°N	100°–0°W	29
North Brazil Current	0°–20°N	70°–40°W	36
Pacific Islands	35°S–30°N	130°E–145°W	29
South China Sea	0°–30°N	99°–125°E	30
Japan/East Sea	34°–48°N	127°–143°E	30
Taiwan	21°–33°N	115°–143°E	35
Tehuantepec	5°–32°N	150°–80°W	30

[21] Prediction error is evaluated by calculating every 6 hours the separation in kilometers between observed and simulated trajectories, starting at 0:00 for each day and continuing over 7 days for each trajectory. Error is zero at 0:00 for the first day of each trajectory. Trajectories are initialized only for the first 359 days of 2003, allowing each to potentially reach its full 7-day extent in 2003. Comparisons are made over periods shorter than 7 days if a drifter ceases transmitting or leaves the evaluation region. Thus, the number of observations used in the statistical calculations tends to decrease as the integration time increases.

5. Results

[22] Results of the drifter comparisons after 24 hours (1 day) and 168 hours (7 days) of integration are summarized in Tables 4 and 5. The evaluation regions are sorted by increasing σ_V. The top-performing experiments are identified by italics, and the percentage of regions for which each experiment was the top- or one of the two top-performing experiments is recorded on the bottom two rows. The final column indicates the number of observed simulated drifter pairs contributing to the regional statistic.

[23] An alternative summary of the comparisons is presented in Figure 5. This is a table of figure panels, sorted into columns of increasing length of trajectory integration (1 and 7 days) and into rows of generally increasing model performance. Each plot compares the results from one of five experiments (persistence, climatology, V2.0, V2.0a, and V2.5a) with the results from the overall best case, V2.5. Each panel also shows a linear fit to the data, which

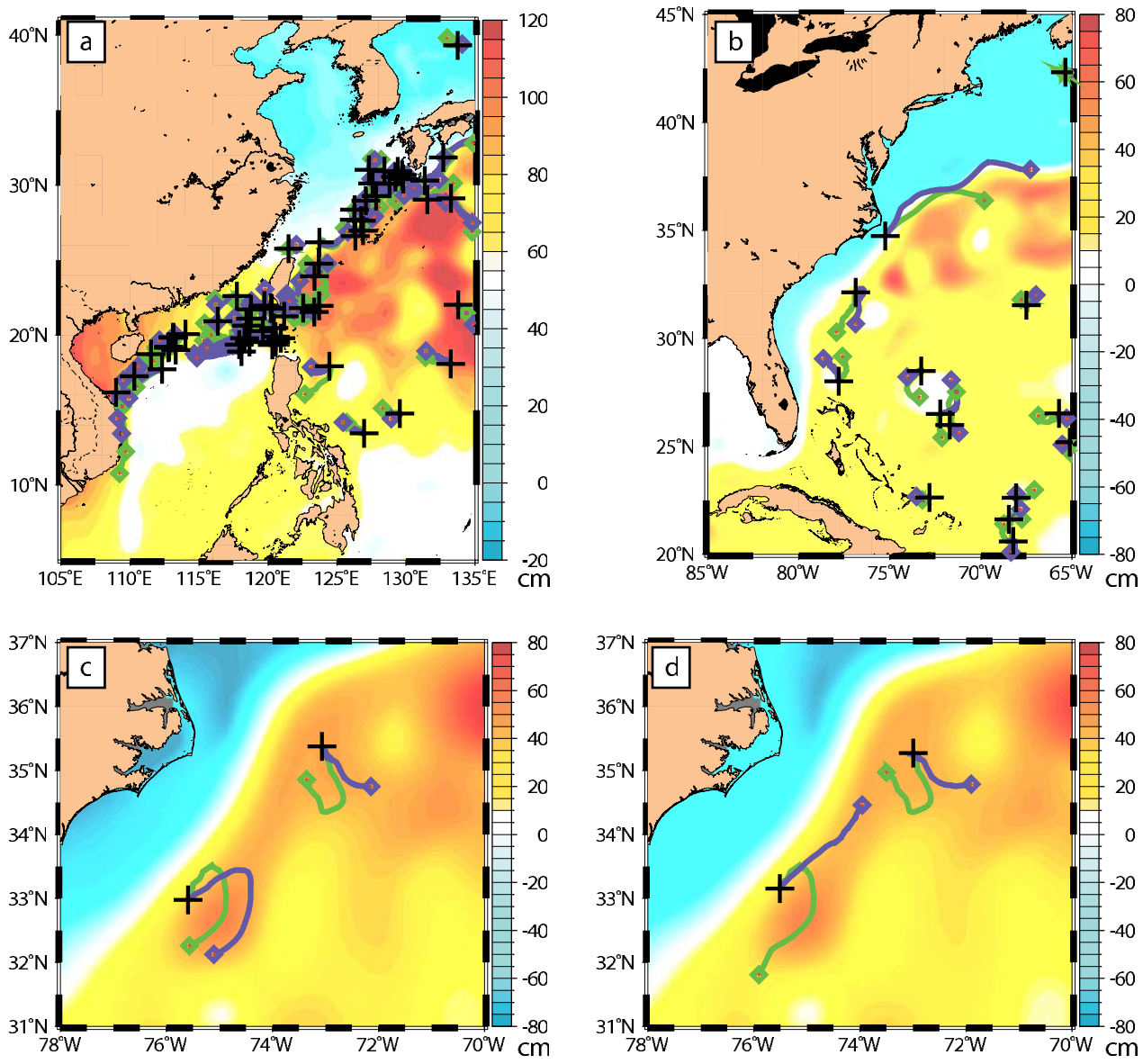

Figure 4. Comparisons between observed drifter trajectories (green) and simulated trajectories (magenta) integrated using 3-hourly NCOM surface velocities from NGOMS V2.5a. A cross marks each starting location, while diamonds indicate each observed or simulated drifter location 7 days later. Panels for the (a) East Asian and (b) Gulf Stream regions show the distribution of 7-day trajectories starting on 10 December 2003. A pair of drifters near the Gulf Stream off Cape Hatteras is shown on consecutive days in Figures 4c (24 January 2003) and 4d (25 January 2003). Trajectory predictions for the northeastern drifter seem highly correlated between the 2 days, while predictions for the southwestern drifter are distinct.

estimates separation error to be proportional to σ_V, the equation for the linear fit, and a square of the correlation coefficient R. A perfect linear fit would have $R^2 = 1$; most of these cases show a generally linear trend with R^2 above 0.6.

[24] The objective of this study is to determine which model configuration leads to the most accurate predictions of drifter motion. The tabulated statistics (Tables 4 and 5) indicate that NCOM from V2.5 most frequently has the smallest or one of the two smallest RMS errors. V2.5 produces the smallest RMS error in 60% of the regions after 1 day and in 40% of the regions after 7 days; it is one of the two best experiments in over 80% of the regions after both 1 and 7 days. In five of six regions with σ_V below 23 cm s^{-1}, V2.0a is the top version after 1 and 7 days. This suggests that the importance of the SSHA correction term is relatively high in regions of lower variability. The SSHA correction alters the mean currents, which is relatively more important if variations about the mean are small.

[25] V2.5 was also not among the top performers in the Kuroshio region; V2.5a produced the smallest errors after both 1 and 7 days. V2.5a performed relatively better in regions with larger σ_V, indicating that both higher-resolution SSH fields from NLOM and an SSHA correction term contributed in these areas. Recall that the correction term

Table 4. RMS Separation (km) After 1 Day Between Observed and Simulated Drifter Trajectories for Model Experiments in 2003[a]

Region	Persist, km	V2.0, km	V2.5, km	V2.0a, km	V2.5a, km	Clim, km	σ_V, cm s^{-1}	n Pairs
Celtic-Biscay-North Sea	16.55	15.53	***13.63***	13.76	*13.68*	16.21	19	2,819
Iberia Region	10.89	11.72	*10.35*	***10.12***	10.36	11.71	19	2,843
Humboldt Current	12.60	11.85	11.29	***10.73***	*11.20*	11.53	21	6,550
Eastern North Pacific	14.75	14.67	12.94	***12.78***	*12.91*	14.38	22	6,420
Brazil Malvinas Confluence	17.81	16.74	15.31	***15.06***	*15.28*	16.77	23	13,349
Gulf of Alaska	13.52	13.90	***12.12***	***12.12***	12.31	13.70	23	2,371
Benguela Current	17.15	16.76	***15.32***	15.89	*15.46*	15.77	24	3,292
Black Sea	17.00	16.96	*16.02*	16.15	***16.01***	16.03	24	1,130
Australia-New Zealand	18.26	16.90	***15.31***	15.40	**15.36**	16.66	25	4,459
Central Pacific	22.20	17.00	*16.13*	***16.06***	16.17	18.68	26	7,855
Gulf of Guinea	18.90	17.40	***16.65***	17.90	17.75	*17.24*	28	5,182
Equatorial Atlantic	16.42	15.14	***14.30***	14.67	14.78	*14.65*	29	15,607
North Atlantic	17.92	17.71	*15.91*	***15.90***	16.06	17.30	29	41,155
Pacific Islands	23.60	18.82	***17.90***	*18.38*	18.44	20.44	29	36,512
Japan/East Sea	21.61	20.82	***18.96***	*19.00*	19.42	19.76	30	1,646
South China Sea	33.63	24.64	***22.40***	23.79	*23.24*	26.95	30	2,793
Tehuantepec	25.50	19.14	***17.82***	*18.05*	18.23	22.10	30	9,537
Equatorial Pacific	24.45	19.18	***18.50***	*18.82*	19.22	20.57	32	44,482
Indian Ocean	25.20	21.67	***19.77***	20.77	*19.90*	25.40	32	15,661
Java Sea	26.75	26.31	*24.87*	26.75	25.92	***24.64***	32	1,039
Intra-Americas Seas	19.67	18.76	***17.20***	17.66	*17.21*	19.13	33	6,250
Agulhas	29.27	24.77	***22.30***	22.70	***22.30***	26.95	34	5,971
East Asian Pacific	32.12	24.20	***22.10***	23.03	*22.43*	25.71	34	5,111
Madagascar	30.62	26.76	*24.77*	25.34	***24.32***	26.29	34	990
Kuroshio	24.67	22.55	20.41	*20.17*	***20.13***	22.44	35	5,456
Taiwan	31.76	24.98	*22.83*	23.15	***21.37***	25.22	35	3,201
North Brazil Current	19.74	17.68	*17.49*	***17.17***	17.80	18.09	36	2,743
Arabian Sea	27.90	23.78	***21.11***	22.50	*21.75*	28.68	38	2,978
Gulf of Mexico	25.53	22.88	***21.32***	22.15	*21.75*	23.58	38	546
Gulf Stream	23.49	22.66	***20.22***	20.76	*20.31*	21.81	38	3,499
Top	***0.00%***	***0.00%***	***60.00%***	***26.67%***	***16.67%***	***3.33%***		
In top 2	*0.00%*	*0.00%*	*86.67%*	*43.33%*	*60.00%*	*10.00%*		

[a]Regions are sorted by increasing σ_V, square root of velocity variance. For each region, the most accurate simulation results are in bold-italic, while the second-place results are in italic. The last two rows summarize relative experiment performance, indicating the percentage of regions in which each experiment produces the best (bold-italic) or one of the two best (italic) sets of results.

used in V2.5a was originally calculated and applied using the 1/16° NLOM for V2.0a. Corrections based directly on the 1/32° NLOM fields have not yet demonstrated sufficient overall performance to be incorporated in the operational systems.

[26] After 7 days, V2.5 fell out of the top pair in four regions that had reported high performance after 1 day: Japan/East Sea, Gulf of Mexico, Java Sea, and North Brazil Current. In the first two of these, V2.5 was the top performer at the 24-hour mark. All have smaller than average sample sizes, with fewer than 1000 pairs in the Gulf of Mexico and Java Sea. In the Japan/East Sea, Java Sea, and Benguela Current, climatology is the top performer after 7 days, indicating that model skill for longer trajectory predictions needs to be improved in these regions. Climatology was the best model only in the Java Sea at the 24-hour comparison.

[27] Why does V2.5 perform relatively poorly in some regions? The SSHA correction appears significant in regions where V2.0a or V2.5a performs best. After both 1 and 7 days, V2.0a yields the most accurate trajectories in the Humboldt, Eastern North Pacific, North Brazil Current, and Brazil-Malvinas Confluence regions. V2.5a has the best performance in the Kuroshio in both cases and in the Gulf of Mexico after 7 days. Higher NCOM resolution is needed to resolve the circulation in the Java and Japan/East Sea.

[28] Figure 5 helps put the comparison statistics in perspective. The panels from top to bottom show a clear progression from a worst case of persistence, somewhat better results using climatological currents, and further improvement using V2.0. While the summary statistics on the bottom lines of Tables 4 and 5 strongly indicate that V2.5 produces the best overall results, the linear regressions in Figure 5 suggest that while V2.5 is the best case, performances of V2.0a and V2.5a are not too far behind. In fact, at the precision shown, the regression curves for V2.5 and V2.5a differ only in the 7-day comparison (Figure 5j), where V2.5a has a slope of 3.30 km s cm^{-1} versus a slope of 3.28 km s cm^{-1} for V2.5. All three cases clearly produce more accurate currents than V2.0.

6. Conclusions

[29] Drifter trajectories simulated in a set of modeling systems are compared with observed trajectories as one aspect of a validation study to determine which alternative, if any, would be the best upgrade for the existing model configuration. What do the evaluation results in Tables 4 and 5 reveal about the relative performance of the initial operational version of NGOMS, V2.0? In the 1-day trajectories, it was no better than third place in any of the 30 evaluation regions; in the 7-day comparisons, it managed to finish in second place twice. V2.0 was never the best case. The results support a decision to upgrade V2.0 with one of the alternatives.

Table 5. RMS Separation (km) After 7 Days Between Observed and Simulated Drifter Trajectories for Model Experiments in 2003[a]

Region	Persist, km	V2.0, km	V2.5, km	V2.0a, km	V2.5a, km	Clim, km	σ_V, cm s^{-1}	*n* Pairs
Celtic-Biscay-North Sea	80.32	68.77	***65.72***	*66.11*	66.24	77.79	19	2,665
Iberia Region	57.44	58.68	*55.69*	***53.71***	55.82	62.92	19	2,636
Humboldt Current	69.03	61.32	62.46	***58.36***	61.69	*60.27*	21	6,081
Eastern North Pacific	78.38	74.80	*70.19*	***68.00***	70.34	76.03	22	6,063
Brazil Malvinas Confluence	94.17	85.73	*81.43*	***79.84***	82.14	85.85	23	12,885
Gulf of Alaska	69.56	68.11	*63.84*	***62.89***	66.20	71.10	23	2,135
Benguela Current	94.56	93.29	*86.28*	89.15	86.47	***83.14***	24	2,984
Black Sea	82.37	78.37	*74.02*	75.81	***73.80***	74.92	24	1,065
Australia-New Zealand	99.67	87.78	*85.20*	85.63	***85.01***	87.00	25	4,240
Central Pacific	134.11	95.09	*92.80*	***91.12***	93.36	105.91	26	7,572
Gulf of Guinea	109.99	*95.20*	***92.22***	103.06	99.38	97.75	28	4,754
Equatorial Atlantic	94.80	82.27	***79.22***	81.66	81.84	*80.91*	29	15,005
North Atlantic	94.32	89.28	*84.23*	***84.06***	84.70	90.35	29	40,273
Pacific Islands	140.85	106.80	***103.28***	*105.76*	106.03	115.74	29	35,335
Japan/East Sea	104.20	95.07	93.12	*92.43*	95.67	***91.88***	30	1,501
South China Sea	188.64	131.29	***123.42***	*128.27*	128.47	152.24	30	2,423
Tehuantepec	150.03	97.79	***91.58***	*91.81*	95.13	123.46	30	8,805
Equatorial Pacific	148.34	107.71	***104.93***	*107.01*	109.66	117.06	32	42,777
Indian Ocean	147.17	125.56	***112.75***	120.26	*113.42*	139.44	32	14,937
Java Sea	143.68	144.97	140.63	148.73	*136.13*	***130.98***	32	817
Intra-Americas Seas	105.91	102.02	*94.75*	99.44	***94.20***	102.79	33	5,853
Agulhas	154.05	124.91	***114.81***	116.71	*114.87*	129.85	34	5,431
East Asian Pacific	182.58	127.44	***120.29***	125.92	*122.82*	140.72	34	4,715
Madagascar	168.12	147.35	*132.31*	137.49	***129.85***	134.52	34	757
Kuroshio	131.71	120.83	114.84	*112.07*	***111.90***	119.03	35	5,086
Taiwan	178.03	136.98	*130.44*	130.67	***124.73***	136.28	35	2,711
North Brazil Current	107.38	*95.43*	96.93	***92.37***	96.95	97.39	36	2,499
Arabian Sea	170.71	140.63	***123.16***	132.14	*126.26*	172.62	38	2,622
Gulf of Mexico	*101.50*	110.91	101.83	110.70	***100.91***	107.91	38	445
Gulf Stream	121.01	114.08	101.60	111.67	*105.08*	110.81	38	3,164
Top	***0.00%***	***0.00%***	***40.00%***	***26.67%***	***23.33%***	***10.00%***		
In top 2	*3.33%*	*6.67%*	*80.00%*	*50.00%*	*43.33%*	*16.67%*		

[a]Regions are sorted by increasing σ_V, square root of velocity variance. For each region, the most accurate simulation results are in bold-italic, while the second-place results are in italic. The last two rows summarize relative experiment performance, indicating the percentage of regions in which each experiment produces the best (bold-italic) or one of the two best (italic) sets of results.

[30] Each of the proposed alternatives, V2.0a, V2.5, and V2.5a, generally produced more accurate predictions of drifter motion than did V2.0, supporting our hypotheses that improved NLOM resolution or more accurate treatment of the ($SSHA_{MODAS}-SSHA_{NLOM}$) within the NGOMS would produce a better operational product. Do the results indicate a preference for one of the alternatives? After 7 days, V2.5 was the top performer in 40% of the regions and among the top two in 80% of the regions. Considering the 1-day trajectories that are more operationally relevant, the relative performance of V2.5 improved: It was the top performer in 60% of the regions and among the top two in 86%. No other version was the top performer in more than 27% of the regions or among the top two in more than 60% of the regions in either the 1-day or the seven-day comparisons. Figure 5 shows that V2.5 has the smallest slope in the linear regression of RMS separation versus σ_V for both 1- and 7-day comparisons. These results, combined with additional studies by NRL and NAVOCEANO not shown here, support the decision to upgrade the operational NGOMS to V2.5. The extensive observational drifter data allowed a robust regional evaluation using simulated drifter trajectories.

[31] While the performance rankings in Tables 4 and 5 indicate a clear preference for V2.5, Figure 5 shows that the performances of V2.0a and V2.5a do not lag far behind. Even though the ($SSHA_{MODAS}-SSHA_{NLOM}$) correction term used in V2.5a did not lead to an overall improvement relative to V2.5, the success of such a correction in improving V2.0a relative to V2.0 suggests that an appropriate correction term could lead to significant improvement. A test case using a preliminary SSHA correction field calculated using the 1/32° NLOM means (not shown) did not perform as well overall as did V2.5a, demonstrating that an insufficiently accurate correction field can do more harm than good. Some work is underway that may lead to a more accurate SSHA correction or alternate methods to produce more accurate synthetic profiles for assimilation into ocean models. Steric height anomalies calculated from historical observations are being paired with SSHA from NLOM or with SSHA from altimeter data processed to remove the nonsteric signal. Additional efforts are underway to produce more accurate synthetic temperature and salinity profiles, providing new capabilities to account for salinity variations independently from temperature variations as suggested by

Figure 5. Summary of RMS separation (in kilometers) after 1 day and 7 days between observed and simulated drifter trajectories for model experiments in 2003. Each panel shows a linear fit to the data, which estimates separation error to be proportional to σ_V, the square root of regional velocity variance. Results fromV2.5, the experiment with the smallest errors overall, are included in each panel for reference.

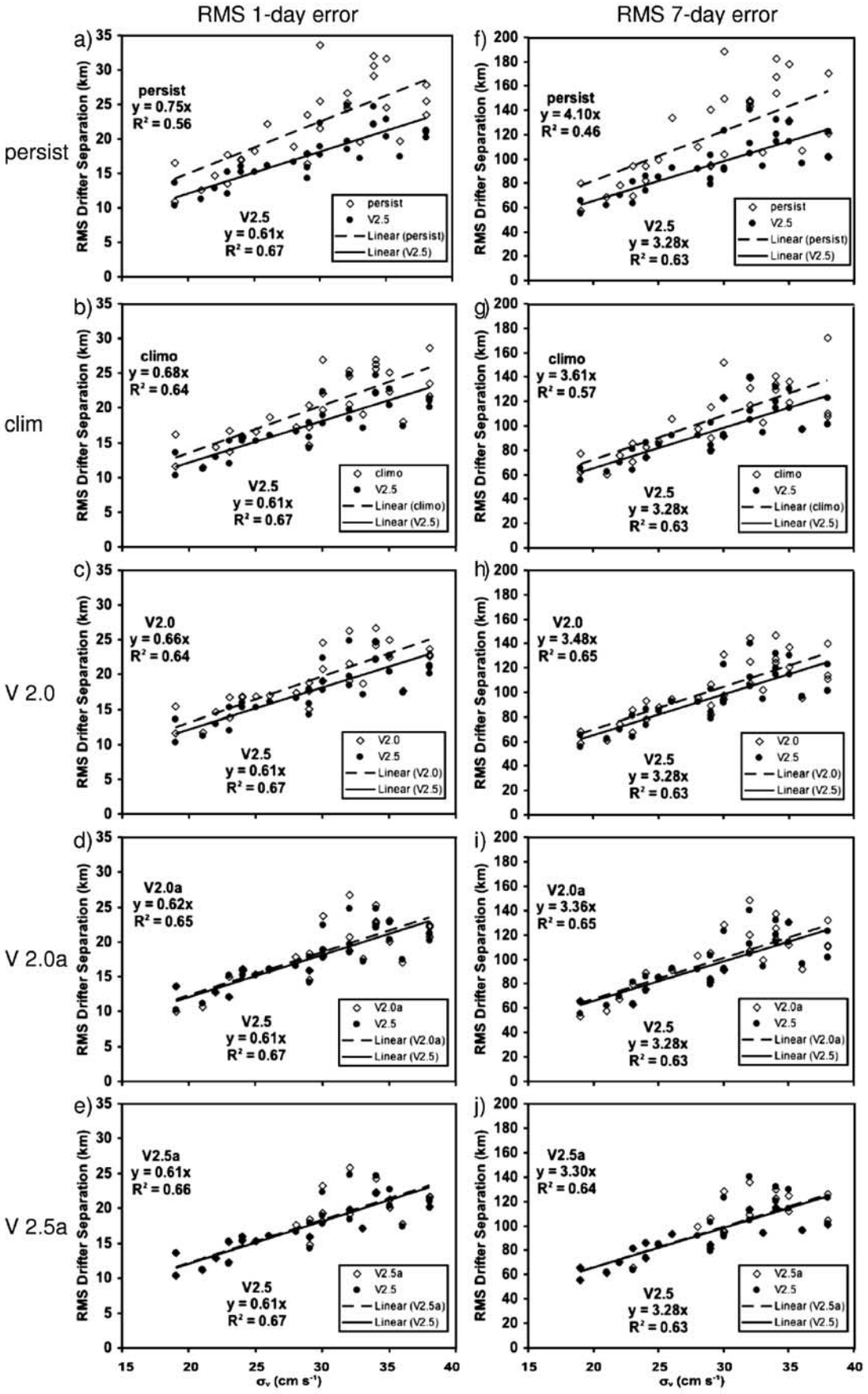
RMS 1-day error
RMS 7-day error
persist
clim
V 2.0
V 2.0a
V 2.5a
a)
b)
c)
d)
e)
f)
g)
h)
i)
j)
RMS Drifter Separation (km)
σv (cm s-1)
persist y = 0.75x R² = 0.56
V2.5 y = 0.61x R² = 0.67
persist y = 4.10x R² = 0.46
V2.5 y = 3.28x R² = 0.63
climo y = 0.68x R² = 0.64
climo y = 3.61x R² = 0.57
V2.0 y = 0.66x R² = 0.64
V2.0 y = 3.48x R² = 0.65
V2.0a y = 0.62x R² = 0.65
V2.0a y = 3.36x R² = 0.65
V2.5a y = 0.61x R² = 0.66
V2.5a y = 3.30x R² = 0.64
Linear (persist)
Linear (climo)
Linear (V2.0)
Linear (V2.0a)
Linear (V2.5a)
Linear (V2.5)

Figure 5

the results for the Alaska Stream. As higher model resolutions, more accurate synthetic profiles, more sophisticated data assimilation, and other system improvements are developed, next-generation systems can be evaluated using simulated and observed drifter trajectories to determine whether or not the new capabilities deliver improved performance.

[32] Prediction of drifter trajectories will always be limited by dynamics unresolved in time and space, such as the phase of inertial oscillations and turbulence in the velocity field. The observed drifter is a sample among many possible outcomes which would result from slight perturbations in time or space. The problem is illustrated by Figure 4d in which the observed and simulated drifter trajectories move in opposite directions. A discussion of two-dimensional turbulence by *Haller and Yuan* [2000] describes that Lagrangian definitions for the boundaries of coherent structures can emerge in turbulence for finite periods of time, unresolved vortices whose impact is better represented by tracer dispersion than single-particle advection. Prediction of drifter fate in subsequent evaluations might be better represented as a probability distribution from a cluster of simulated drifters, each seeded with slightly perturbed seed time and initial location. Similarly, large numbers of drifter observations are required for evaluations since a single trajectory realization may not be a good indication of the most likely fate of a cluster of drifters.

[33] **Acknowledgments.** This publication is a contribution to the Improved Synthetic Ocean Profiles initiative supported by the Office of Naval Research under program element 602345N. Numerical simulations for this effort were supported under the Department of Defense High Performance Computing Modernization Program on an IBM SP3 at the Naval Oceanographic Office, Stennis Space Center, Mississippi. We thank LCDR Karen Ebersole for her contributions to initial drifter comparisons within the U.S. Naval Reserve program. We also thank Harley Hurlburt, Birol Kara, and Jay Shriver for their valuable guidance and the anonymous reviewers for their thorough examination and constructive comments. This is contribution NRL/JA/7320/2006/7001 and has been approved for public release.

References

Barron, C. N., and A. B. Kara (2006), Satellite-based daily SSTs over the global ocean, *Geophys. Res. Lett.*, *33*, L15603, doi:10.1029/2006GL026356.

Barron, C. N., A. B. Kara, H. E. Hurlburt, C. Rowley, and L. F. Smedstad (2004), Sea surface height predictions from the global Navy Coastal Ocean Model (NCOM) during 1998–2001, *J. Atmos. Ocean. Technol.*, *21*, 1876–1894.

Barron, C. N., A. B. Kara, P. J. Martin, R. C. Rhodes, and L. F. Smedstad (2006), Formulation, implementation and examination of vertical coordinate choices in the global Navy Coastal Ocean Model (NCOM), *Ocean Model.*, *11*, 347–375, doi:10.1016/j.ocemod.2005.01.004.

Boebel, O., and C. Barron (2003), A comparison of in-situ float velocities with altimeter derived geostrophic velocities, *Deep Sea Res. II*, *50*, 119–139.

Chen, S., and E. Firing (2006), Currents in the Aleutian Basin and subarctic North Pacific near the dateline in summer 1993, *J. Geophys. Res.*, *111*, C03001, doi:10.1029/2005JC003064.

Fratantoni, D. M. (2001), North Atlantic surface circulation during the 1990's observed with satellite-tracked drifters, *J. Geophys. Res.*, *106*, 22,067–22,093.

Fox, D. N., W. J. Teague, C. N. Barron, M. R. Carnes, and C. M. Lee (2002), The Modular Ocean Data Assimilation System (MODAS), *J. Atmos. Ocean. Technol.*, *19*, 240–252.

Haller, G., and G. Yuan (2000), Lagrangian coherent structures and mixing in two-dimensional turbulence, *Physica D*, *147*, 352–370.

Hansen, D., and A. Herman (1989), Temporal sampling requirements for surface drifting buoys in the tropical Pacific, *J. Atmos. Ocean. Technol.*, *6*, 599–607.

Hansen, D., and P.-M. Poulain (1996), Quality control and interpolations of WOCE-TOGA drifter data, *J. Atmos. Ocean. Technol.*, *13*, 900–909.

Hurlburt, H. E., and P. J. Hogan (2000), Impact of 1/8 degrees to 1/64 degrees resolution on Gulf Stream model—Data comparisons in basin-scale subtropical Atlantic Ocean models, *Dyn. Atmos. Ocean.*, *3–4*, 341–361.

Kara, A. B., C. N. Barron, P. J. Martin, L. F. Smedstad, and R. C. Rhodes (2006), Validation of interannual simulations from the 1/8° Global Navy Coastal Ocean Model (NCOM), *Ocean Model.*, *11*, 376–398, doi:10.1016/j.ocemod.2005.01.003.

Lugo-Fernandez, A., K. J. P. Deslarzes, J. M. Price, G. S. Boland, and M. V. M. V. Morin (2001), Inferring probable dispersal of Flower Garden Banks coral larvae (Gulf of Mexico) using observed and simulated drifter trajectories, *Cont. Shelf Res.*, *21*, 47–67.

Lumpkin, R., and M. Pazos (2007), Measuring surface currents with Surface Velocity Program drifters: The instrument, its data, and some recent results, chap. 2, *Lagrangian Analysis and Prediction of Coastal and Ocean Dynamics* (*LAPCOD*), edited by A. Griffa, A. D. Kirwan, A. J. Mariano, T. Özgökmen, and T. Rossby, 520 pp., Cambridge Univ. Press, New York.

Naimie, C. E., R. Limeburner, C. G. Hannah, and R. C. Beardsley (2001), On the geographic and seasonal patterns of the near-surface circulation on Georges Bank—From real and simulated drifters, *Deep Sea Res. II*, *48*, 501–518.

Niiler, P. P., A. Sybrandy, K. Bi, P. Poulain, and D. Bitterman (1995), Measurements of the water-following capability of holey-sock and TRISTAR drifters, *Deep Sea Res.*, *42*, 1951–1964.

Özgökmen, T. M., A. Griffa, A. J. Mariano, and L. I. Piterbarg (2000), On the predictability of Lagrangian trajectories in the ocean, *J. Atmos. Ocean. Technol.*, *17*, 366–383.

Özgökmen, T. M., L. I. Piterbarg, A. J. Mariano, and E. H. Ryan (2001), Predictability of drifter trajectories in the tropical Pacific Ocean, *J. Phys. Oceanogr.*, *31*, 2691–2720.

Poulain, P.-M. (1999), Drifter observations of surface circulation in the Adriatic Sea between December 1994 and March 1996, *J. Mar. Sys.*, *20*, 231–253.

Press, W. H., B. P. Flannery, S. A. Teukolsky, and W. T. Vetterling (1986), *Numerical Recipes: The Art of Scientific Computing*, 818 pp., Cambridge Univ. Press, New York.

Rhodes, R. C., et al. (2002), Navy real-time global modeling systems, *Oceanography*, *15*, 29–43.

Reverdin, G., P. P. Niiler, and H. Valdimarsson (2003), North Atlantic Ocean surface currents, *J. Geophys. Res.*, *108*(C1), 3002, doi:10.1029/2001JC001020.

Shriver, J. F., and H. E. Hurlburt (2000), The effect of upper ocean eddies on the non-steric contribution to the barotropic mode, *Geophys. Res. Lett.*, *27*, 2713–2716.

Shriver, J. F., H. E. Hurlburt, O. M. Smedstad, A. J. Wallcraft, and R. C. Rhodes (2007), 1/32° real-time global ocean prediction and value-added over 1/16° resolution, *J. Mar. Sys.*, 3–26, doi:10.1016/j.jmarsys.2005.11.02.

Smedstad, O. M., H. E. Hurlburt, E. J. Metzger, R. C. Rhodes, J. F. Shriver, A. J. Wallcraft, and A. B. Kara (2003), An operational eddy-resolving 1/16° global ocean nowcast forecast system, *J. Mar. Sys.*, *40–41*, 341–361.

Teague, W. J, M. J. Carron, and P. J. Hogan (1990), A comparison between the Generalized Digital Environmental Model and Levitus climatologies, *J. Geophys. Res.*, *95*, 7167–7183.

Thompson, K. R., J. Sheng, P. C. Smith, and L. Cong (2003), Prediction of surface currents and drifter trajectories on the inner Scotian Shelf, *J. Geophys. Res.*, *108*(C9), 3287, doi:10.1029/2001JC001119.

Vastano, A. C., and C. N. Barron (1994), Comparison of satellite and drifter surface flow estimates in the northwestern Gulf of Mexico, *Cont. Shelf Res.*, *14*, 589–605.

Wallcraft, A. J., A. B. Kara, H. E. Hurlburt, and P. A. Rochford (2003), The NRL Layered Global Ocean Model (NLOM) with an embedded mixed layer sub-model: Formulation and tuning, *J. Atmos. Ocean. Technol.*, *20*, 1601–1615.

Zhurbas, V., and I. M. Oh (2003), Lateral diffusivity and Lagrangian scales in the Pacific Ocean as derived from drifter data, *J. Geophys. Res.*, *108*(C5), 3141, doi:10.1029/2002JC001596.

C. N. Barron, J. M. Dastugue, and L. F. Smedstad, Naval Research Laboratory, Stennis Space Center, MS 39529, USA. (charlie.barron@nrlssc.navy.mil)

O. M. Smedstad, Planning Systems Incorporated, Stennis Space Center, MS 39529, USA.